*Proceedings of the 19th National Conference on Superconductivity, Bronisławów, Poland, October 6–11, 2019*

# Dynamic Transport Critical Current Measurements of $MgB_2$ Superconductor

B.A. Glowacki [a,b,c,*] and M. Wozniak[d]

[a] *Institute of Power Engineering, Mory 8, 01-330 Warsaw, Poland*
[b] *Department of Materials Science and Metallurgy, University of Cambridge, 27 Ch. Babbage Road, Cambridge CB3 0FS, UK*
[c] *Department of Physics and Energy, Bernal Institute, University of Limerick, Castletroy, Ireland*
[d] *Siemens MR Magnet Technology, Eynsham, OX29 4BP, UK*

Doi: 10.12693/APhysPolA.138.695 *e-mail: bag10@cam.ac.uk

Measurements of transport critical current of superconducting conductors with respect to temperature and magnetic field are of particular importance for medical and energy applications. The main interest of using the superconducting materials such as $MgB_2$, Bi-based and $YBa_2Cu_3O_7$ is in the range of 4–40 K and testing facilities covering such a range of temperatures and magnetic fields can be costly, especially when considering the cooling power required in the cryogenic system and also a dramatically growing cost of liquid helium and its shortage. Transport critical currents in excess of 1000 A at temperatures above LHe are common for commercial wires, making the testing of such samples difficult in setups cooled via a cryocooler even by force gas cooling. There is also a fundamental interest in the study of superconducting conductors in magnetic fields higher than $B = 20$ T; such magnetic flux density can be obtained by using pulse techniques, however data interpretation can be difficult and there are some potential discrepancies. In the current paper we present how improved stepwise pulse current and signal averaging procedure combined with stepwise pulse transport current and flat-top pulse magnetic field measurements can deliver results identical to the combined DC transport current and DC magnetic field in milliseconds and also with a minimum boil-off of helium.

topics: pulse transport critical current measurements, $MgB_2$, flux dynamics

## 1. Introduction

The growing price of LHe [1, 2] and a shortage of this important cryogenic liquid (see Fig. 1) stimulate research towards a more economical way to conduct transport current characterization of the technical conductors for applications at a low temperature range. The conventional method, widely applied and recognized as the standard measurement method, uses constant (time-invariant) magnetic field and only slowly-varying electric current. Measurements with this constant field and the direct transport current (CF/DC) method can be performed accurately and reproducibly. The problem, however, is that such a measurement usually requires long time at LHe and ohmic losses from the current leads and actual terminals cause an unacceptable evaporation rate of LHe per sample. If there is lack of the full He recovery system in place, such measurements are prohibitively expensive.

In our earlier work, we proposed a pulse transport current measurement that can be a solution as a low-cost measurement procedure [3, 4]. Following an earlier pioneering work the fully operational Cryo-BI-Pulse system configuration has been developed [5] based on a capacitor bank (CB) discharge as the source of the transport current through a magnet coil and the wire and CB-PF/CB-PC.

The main objective of the work is to improve the accuracy of CB-PF/CB-PC measurements in which the main limitation is the duration of the magnetic field pulse plateau, flat-top [6, 7]. The magnetic field during the plateau remains constant (+0.3 to −0.5% of the mean value) for 4 ms from 5 ms after the pulse has been triggered. This defines the measurement time frame and indicates the need to use more sophisticated data acquisition and analysis than the one used in the constant field direct current (CF/DC) technique. The latter techniques are typically used as reference points for assessing the accuracy of all presented pulse field and pulse current measurement methods. With such, the $J_c$ values of the sample correspond to the $I_c$ values divided by the cross-sectional area of the superconducting core. The $I_c(B)$ was, however, assessed by two methods in two different systems which mainly differ by the rate of current and field variation in time and the duration of the measurement as well.

## 2. Pulse method

### 2.1. Method description

The CF/DC method is widely recognized as the standard measurement method and uses constant (time-invariant) magnetic field and only slowly-varying electric current. Measurements in such conditions can be performed accurately and reproducibly. The pulse method, which will be the main subject of this paper, applies both the pulsed magnetic field and the pulse electric current to the sample as described below. The pulse method systems and results will be discussed for three different variants of current pulsing methodology:

- capacitor bank discharge pulse field/capacitor bank discharge pulse current CB-PF/CB-PC,
- capacitor bank discharge pulse field/power supply pulse current CB-PF/PS-PC,
- capacitor bank discharge pulse field/power supply stepwise pulse current CB-PF/PSS-PC.

All $I_c$ measurements were performed on straight pieces of $MgB_2$ wire by a standard four-point transport method, in a liquid helium bath (4.2 K) and with the sample length (and current direction) perpendicular to the magnetic field, Fig. 2a and b.

Measurements were performed on the *in situ* $MgB_2$/Glidcop wire, Fig. 2c (inset), with diameter of 0.79 mm, heat-treated with the optimised sintering parameters of 700 °C for 5 min, Fig. 2c [8].

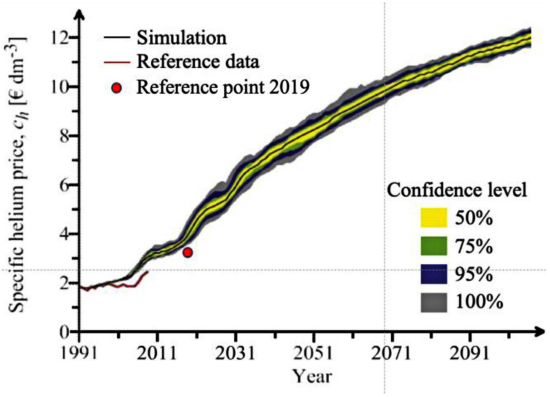


Fig. 1. Prognosis for the average price of helium for the next 110 years. The price is an output of coupled, multi-variable Monte Carlo helium market simulation [1]. The overall future price of helium is expected to rise due to an increase in production costs and, later, the increasing scarcity of helium resources, although the analysis suggests that there is no imminent depletion of economical helium resources before 2060. Original data for gaseous helium in [1] were recalculated to correspond to €per dm$^3$ of liquid helium but no cost of liquefaction has been added. The red dot represents a reference point for 2019.

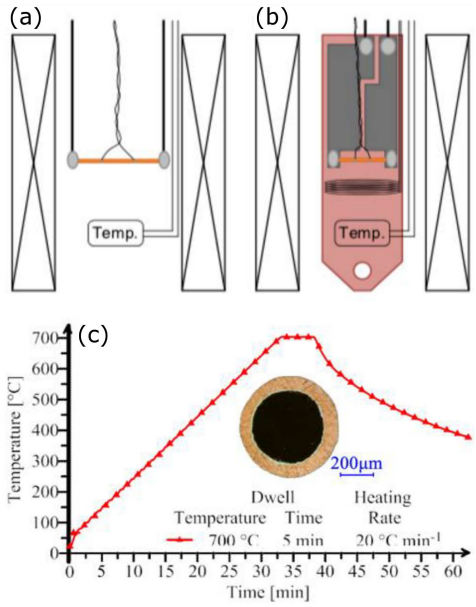


Fig. 2. Schematic of the standard four-point transport measurements method in (a) CFDC, (b) current pulsing techniques, (c) temperature profile of the $MgB_2$ wire heat treatment (the inset, optical micrograph shows the wire cross-section).

### 2.2. Constant field direct current measurements: CF/DC

The CF/DC critical current measurements were performed in the bore of Bitter electromagnets in the International Laboratory of High Magnetic Fields and Low Temperatures, ILHMFLT, Wrocław, Poland. Two Bitter magnets were used: BM1 with a maximum flux density, $B$ of 8 T in a 36 mm diameter cryostat, and BM2 with a maximum $B = 14$ T and a 19 mm diameter cryostat [9].

$MgB_2$ wire samples were 17–18 mm long with voltage contacts soldered 7 mm apart. Current was delivered by a current supply with a maximum current of 150 A and a ramp rate of 2 A/s. A carbon ceramic thermometer was placed directly above the sample to verify a liquid helium immersion. The thermoelectric voltage in the measured sample voltage was cancelled by subtracting the value when the sample current was still zero. The values of $I_c$ were obtained by applying a 1 $\mu$V/cm electric field criterion to the measured $E$–$I$ curves. The $n$-values were obtained by fitting the curve to the measured data with the Levenberg–Marquardt method in the region of $E$ from 1 to 10 $\mu$V/cm. The curve was calculated with

$$E_s = E_c \left( \frac{J_s}{J_c} \right)^n , \qquad (1)$$

where $E_s$ is the electric field in a superconductor, $E_c$ is the critical electric field (for determination of the critical current, usually $E_c = 1$ $\mu$V/cm), $J_c$ is the critical current density, $J_s$ is the electric current density in a superconductor (when voltage along the superconductor appears due to a flux motion

which — up to some level of $J_s$ — can be quite precisely described by a power law) and $n$ is the number often called the $n$-value.

In the next section, the pulsed field and pulsed current measurement results obtained with two experimental configurations and analytical approaches are presented.

### 3. Cryo-BI-Pulse, pulsed field pulsed current measurements: CB-PF/CB-PC

The results of CB-PF/CB-PC measurements with the Cryo-Bi-Pulse system configuration are presented in Fig. 3. The sample holder can only accommodate small-diameter samples soldered to the copper tracks on a printed circuit board as shown in Fig. 4. The maximum sample length for the orientation perpendicular to the magnetic field is limited by the internal diameter of the cryostat (14 mm) which was inserted into the bore of a 30 T pulse magnet (Fig. 3a). The typical samples were 12 mm with $\approx$ 4 mm voltage contacts spacing, see Fig. 4a. Before the insertion into the cryostat, the sample and the current and voltage leads were covered with GE varnish (Fig. 4b) for electrical insulation from the walls of the cryostat and to minimise wire movement during magnetic field pulses. A relative polarity/direction of $B$ and $I$ was chosen to secure the Lorentz force acting on the wire perpendicular towards the sample holder.

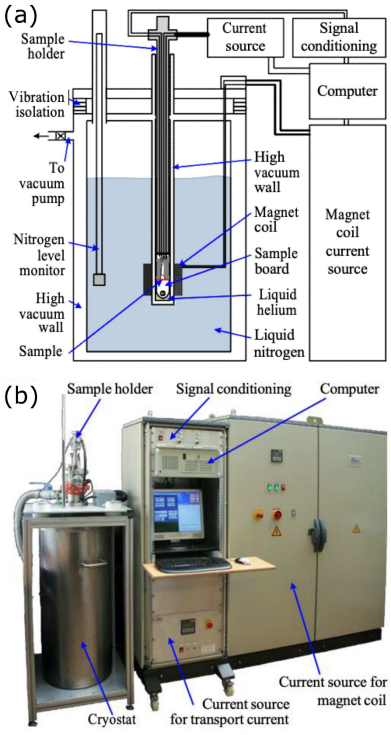


Fig. 3. The Cryo-BI-Pulse system (CB-PF/CB-PC) used for pulsed field pulsed current critical current measurements: (a) general schematic diagram, (b) photograph with basic components marked [5].

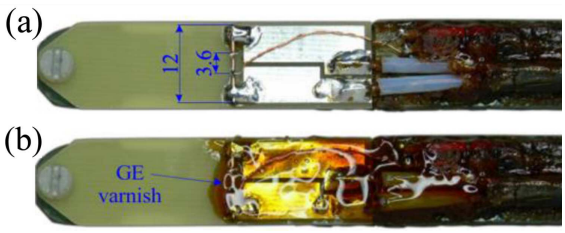


Fig. 4. Photograph of the sample holder with an attached $MgB_2$ wire sample: (a) length of the sample and the distance between the voltage taps in mm, (b) sample covered with GE varnish.

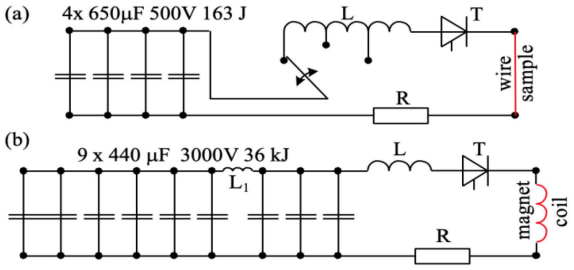


Fig. 5. Simplified circuit diagram of the Cryo-BI-Pulse sources CB-PF/CB-PC for: (a) capacitor bank pulsed current, (b) capacitor bank magnetic field. Pulses are switched on by thyristors, T, and the values of the elements in these RLC circuits define the shapes and durations of the pulses.

Figure 3a presents a schematic diagram with the main components: a liquid helium cryostat with a liquid nitrogen cooled shielding and a resistive pulse coil, sources of current for the sample and pulse coil and a computer for the control and data logging using a multifunction data acquisition card. This system (Fig. 3b) delivers magnetic fields up to 26 T (with a flat top field shape, 16.4 ms long pulse) and current up to 700 A (3.8 ms long pulse) by the discharges of two capacitor banks. One capacitor bank is used for sample current (Fig. 5a) and another one for the magnetic field (Fig. 5b).

The original Cryo-Bi-Pulse system was configured to deliver a current pulse during the plateau of magnetic field by triggering it 5.5 ms after the field pulse has been triggered, see Fig. 6. The 3.8 ms long current pulse is not sinusoidal in shape and reaches its amplitude, only after 1.24 ms. During a magnetic field pulse (Fig. 6, black line), a relatively short current pulse (Fig. 6, blue line) is discharged through the sample and the voltage response is conditioned and recorded by the acquisition system. Ideally, the voltage response for all pulsed currents with an amplitude below $I_c$ has a shape like the green line in Fig. 6 (shown here at 1 T and $I_c = 39.64$ A). In fact, the shape scales with the amplitude of the current pulse. Voltage responses for currents above $I_c$ have shapes like the red curve in Fig. 6. In this case, $I_c$ is determined from the change of shape of the voltage response from

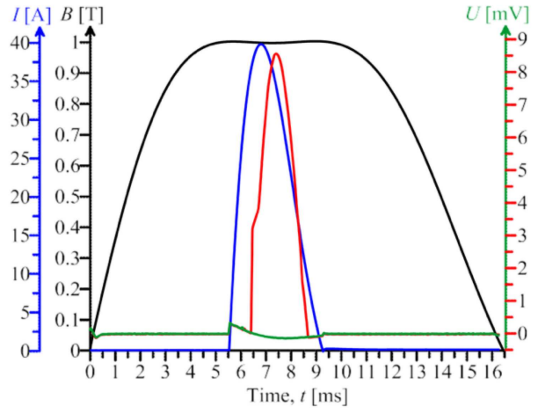


Fig. 6. Timing and typical shapes of pulsed field (amplitude 1 T — black line), pulsed currents (amplitudes 39.64 A and 39.79 A — both blue line) and the voltage responses (without transition — green line and with transition — red line) for a small diameter $MgB_2$ wire at 4.2 K.

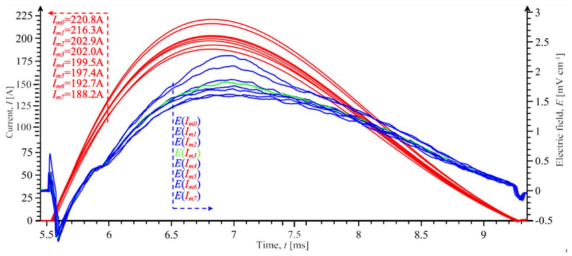


Fig. 7. Sample current (red lines — left ordinates) and sample electric field (blue lines — right ordinates) vs. time. The green curve is interpreted as the first electric field response which contains traces of the transition of the sample to the normal state. The actual change of the shape of the "sin-like" $E$ curves is manifested for currents above 202 A. Next value of 202.9 A is a clear indication of the "resistive-like" $E$ transition observed for higher currents values. The magnetic field pulse is not shown but it was triggered at $t = 0$ s and had an amplitude of 1 T.

wire. For $MgB_2$ wires, this voltage response changes shape quite drastically for current pulses with the amplitude only slightly above $I_c$, and therefore, precise values of the $I_c(B)$ can be obtained.

The voltage signals from a $MgB_2$ wire are presented with some subjectivity of the method of $I_c$ determination. The capacitive discharge pulsed current source used in the Cryo-BI-Pulse system, although allowing very high current pulses up to 700 A, seems not to be fully exploiting the potential of the rest of the system. The three main disadvantages of this pulsed current source are: the difficulty in obtaining two current pulses with exactly the same amplitude, as the capacitor charging voltage is not controlled precisely enough, the inability to change the current shape (e.g. to a linear ramp) and finally the fact that the longest current pulse achieves its maximum after only 1.24 ms. This means that only around 30% of the time during which the magnetic field has a relatively constant value due to its flat top (Fig. 6) is used for current pulse and voltage evaluation.

### 3.1. Data processing

To obtain $I_c$ at a given magnetic field, a series of current pulses of different amplitudes is delivered during magnetic field pulses with a constant amplitude. For clarity, Fig. 7 shows current pulses (red line) only with amplitudes very close to $I_c$ and delivered during the plateau of a 1 T magnetic field pulse. The determination of $I_c$ has been done by comparing qualitatively the shape of the electric field vs. time responses of the sample (blue lines) to a series of these current pulses. In this case, signs of the transition to the resistive state appear in the sample (Fig. 7, green line) for an amplitude of pulsed current equal $I_{m3} = 202$ A. In the case of such PFPC measurements, $I_c$ is defined as the maximum value of pulsed current amplitude for which no sign of resistive transition was observed. For the investigated sample at 1 T and 4.2 K one obtains $I_{m4} = 199.5$ A.

Now, it is apparent that the shape of the electric field vs. time responses from the $MgB_2$ wire samples is changing insignificantly for current pulses with an amplitude only slightly above $I_c$. This makes the $I_c$ determination very subjective and requires a considerable amount of measurement time to obtain many closely-spaced pulses in the current range where the curves begin to change shape.

It should also be noted that in Fig. 7 the electric field $E$ is large [mV/cm] and most of this signal is not caused by the sample response to the pulsed current but by induced voltages in the voltage measurement loop. The near-sinusoidal current pulse shape also means that the rate of change of current, and hence the induced voltage, is time-dependent, further complicating the analysis. The sample self-inductance is also dependent on the current and its rate of change and this contributes to the change of the voltage loop inductance in a complex way.

During or after the measurements, the $E(t)$ curves (Fig. 7) can be recalculated into other related quantities. A plot of electric field vs. sample current, i.e., $E(I)$, is not very useful due to the contribution of induced voltages. In the case of static resistance vs. time, i.e., $r(t)$, curves are obtained by dividing the sample voltage $u(t)$ by the sample current $i(t)$. These curves of $r(t)$ have then shapes which barely change with the amplitude of the pulsed current, until the $I_c$ value is exceeded (Fig. 8). Thus, it is much easier to recognise that the green curve $r(I_{m3})$ starts to deviate from the shape of curves for lower values of pulsed current amplitude $(I_{m4} - I_{m7})$. As in the previous case, the current $I_{m4}$ with an amplitude of 199.5 A is chosen to be the $I_c$ of the sample.

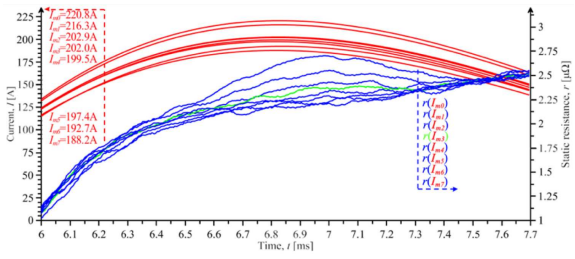


Fig. 8. Sample current (red lines — left ordinates) and sample static resistance $r(t) = u(t)/i(t)$ (blue lines — right ordinates) vs. time. The green curve is interpreted as the first static resistance response which contains traces of the transition of the sample to the normal state. The magnetic field pulse is not shown but it was triggered at $t = 0$ s and had an amplitude of 1 T.

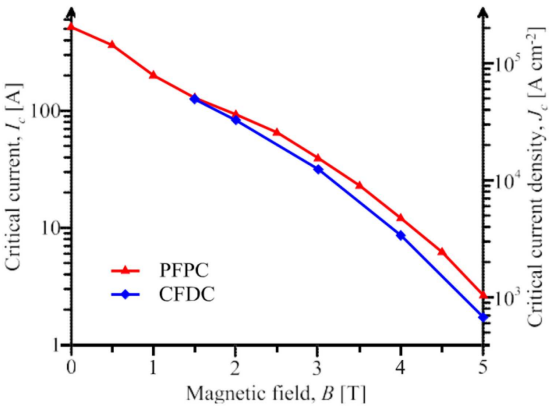


Fig. 9. Comparison of the $I_c(B)$ (left ordinate) and $J_c(B)$ (right ordinate) at 4.2 K obtained from CFDC and CB-PF/CB-PC measurements for the $MgB_2$ wire heat treated at 700 °C for 5 min.

Please note that it is very difficult to create a more sophisticated critical current analysis algorithm since the capacitive discharge current source does not allow for a precise control of the amplitude of the pulsed current and two identical sequential current pulses cannot be obtained, as might be used for differential signal analysis.

### 3.2. Results and discussion

The Cryo-BI-Pulse system with the original configuration allowed the measurements of $I_c$ of samples in the high current region, above the 150 A current limit of the DC current source in ILHMFLT. In CB-PF/CB-PC measurements at 4.2 K and in self-field, the sample investigated here achieved $I_c = 525$ A. For a wire diameter of 0.79 mm, this suggests $J_c = 2 \times 10^5$ A/cm$^2$ (for a filling factor of $\approx 52\%$). The engineering critical current density, $J_e$, in self-field is also high, reaching a value of $1.1 \times 10^5$ A/cm$^2$. The $I_c(B)$ plot obtained from CB-PF/CB-PC measurements (red triangles) for this wire is compared in Fig. 9 to the results obtained with the standard CF/DC method (blue diamonds).

The agreement between the F/DC and CB-PF/CB-PC measurements is quite good, in particular (see Fig. 9), a very close match of $I_c$ appears at 1.5 T, while at lower fields the PFPC measurements plausibly extend the measurement range of the CF/DC method. The discrepancy between the methods increases with increasing magnetic field and is caused by the following reasons. In the CB-PF/CB-PC method $I_c$, determination requires current pulses which are a few amperes higher than $I_c$. This necessity of overshooting by a few amperes to notice signs of the sample transition to a resistive state causes a substantial error when $I_c$ of the sample drops to a similarly low level at higher magnetic fields. This behavior is amplified by the decreasing $n$-value of the measured wire with increasing magnetic field which makes the transitions to the resistive state less sharp and more difficult to identify with the signal analysis method described above. Finally, it should be noted that the CB-PF/CB-PC technique uses different $I_c$ criteria than the CF/DC, defining $I_c$ on a much different electric field scale. The qualitative nature of this analysis and the contributions of variable and induced voltages means that a low and strictly defined electric field criterion could not be applied. With this method it is also very difficult to obtain $n$-values for the measured sample.

## 4. CB-PF/PS-PC measurement technique

This section describes an experimental setup and results obtained with a modified, CB-PF/PS-PC system configuration, where a more flexible and controllable pulsed current source was implemented. The introduction of such a modified technique aims to help obtain more objective results, using current pulses with different shapes and also refined data analysis. The decision was to use KEPCO (Flushing, NY, USA) power supplies which have a very impressive transient operation specification, with a minimum rise or fall time of 35 $\mu$s (10–90% $I_{max}$) [10]. These supplies, when controlled by an arbitrary waveform generator (Agilent 33220A, Fig. 10), allow extremely high flexibility with the pulse current shape and timing but with a maximum continuous or pulsed current limited to 92 A. The primary focus of the work is on improving the accuracy of the CB-PF/PS-PC measurement. For the measurements reported in this section, the capacitive discharge current source used previously has been replaced by a current source capable of delivering accurately any arbitrary shape and duration of current pulse. This current source is limited to 92 A, therefore — to allow measurements in the low field region — a small diameter wire sample was prepared and measured by the CF/DC method to obtain reference data. The main achievement of the work reported here is

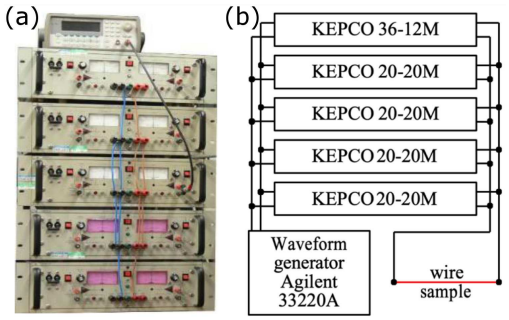


Fig. 10. Newly configured CB-PF/PS-PC, flexible pulsed current source consisting of five power supplies (4× KEPCO-20-20M + 1× KEPCO-36-12M) connected in parallel to achieve 92 A (4 × 20 A +12 A) output current and controlled from the arbitrary waveform generator.

the application of a regression analysis to the electric field vs. current response to allow $I_c$ to be determined using a $E = 1$ $\mu$V/cm criterion. This was possible thanks to the ability to control very accurately the current pulses. The analysis of measurements using sinusoidal and linear current pulses is presented in Sects. 4.1 and 4.2. In Sect. 5, a more sophisticated stepwise current shape was applied and this simplified the analysis of the data obtained from the measurement. The new power supply also allowed for the length of the current pulse to be increased to 4 ms, utilizing the whole duration of the pulsed magnetic field plateau. In combination with the lower peak current, this brings the current ramp rate during the CB-PF/PS-PC measurements closer to the current ramps used during the CF/DC measurements. The increased measurement time also means that during the current pulse more data points are collected and as a result a more aggressive and effective digital noise filtering can be applied. The remaining differences between the refined CB-PF/PS-PC and CF/DC measurements are discussed in the last section and future studies are suggested.

### 4.1. Linear and sinusoidal current ramps

Current pulses 4 ms long were triggered 5 ms after the magnetic field pulse had been triggered, resulting in the magnetic field and current timings shown in Fig. 11. Two different current pulse shapes were used. The first is a linear current increase which resulted in current ramp rates constant over time but dependent on the pulse amplitude. For the maximum pulsed current amplitude, the rate was 92 A/4 ms = 23 kA/s. The second pulse shape is sinusoidal, resulting in a time-varying current ramps rate decreasing to zero as the pulsed current approaches its amplitude (Fig. 11). The use of longer current pulses not only means a lower current ramp rate for the same amplitude of current but also more data points collected during the current pulse for the same data acquisition speed.

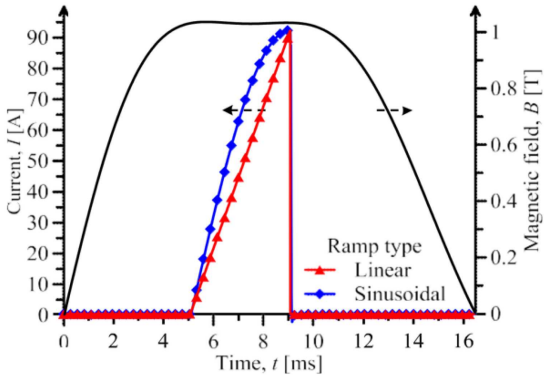


Fig. 11. Magnetic field and current pulses used for testing.

The acquisition system in all CB-PF/PS-PC measurements used recorded data with a 250 kHz sampling rate. With the capacitor discharge pulse duration of the old system, this allowed only ≈ 310 data points to be collected by the time the sample current reached its maximum. In the case of the new power supply with 4 ms current pulses, 1000 data points of each signal of voltage and current could be collected from every current pulse. This allowed digital noise averaging over a larger number of points and, as a result, the processed signals are less noisy.

### 4.2. Data processing

Two types of voltage signal were recorded from the voltage taps of the sample placed in liquid helium and in the pulse magnet before proceeding to the actual $I_c(B)$ measurements. Firstly, the voltage response to a series of current pulses with increasing amplitude and without a magnetic field pulse was recorded as a reference signal which corresponds to the voltage induced by the change of the sample current in time. Secondly, the voltage response to a series of magnetic field pulses with an increasing amplitude (without a sample current pulse) was recorded as a reference signal which corresponds to the voltage induced by the change of the magnetic field in time. These two signals were subtracted from the voltage signal recorded from the sample during the actual measurements, considering the amplitude of the sample current and the pulsed magnetic field. For example, from the electric field of the sample (solid triangles and diamonds in Fig. 12), due to a current pulse with an amplitude of 92 A (solid circles and rectangles in Fig. 12) during a magnetic field pulse with 1 T plateau (see Fig. 11), the sample voltage responses to a 92 A current pulse without magnetic field (open triangles and diamonds in Fig. 12) and to 1 T magnetic field pulse without sample current were subtracted. The last signal was generally very close to zero due to the use of a compensation coil in the Cryo-BI-Pulse system to remove a large portion of the voltage induced by the pulsed magnetic field.

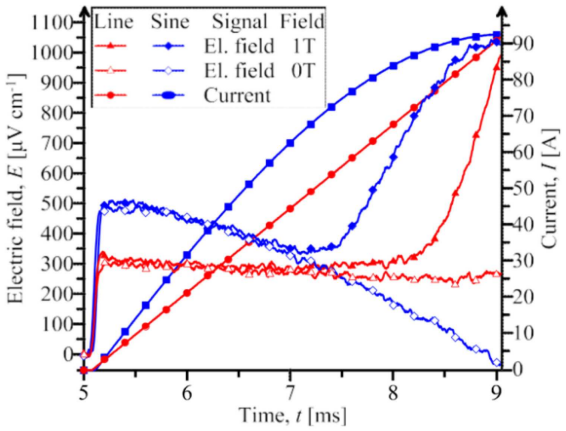


Fig. 12. Electric field (left ordinate) signals recorded from the sample during sinusoidal and linear current pulses (right ordinate) at 0 T and with a 1 T magnetic field pulse.

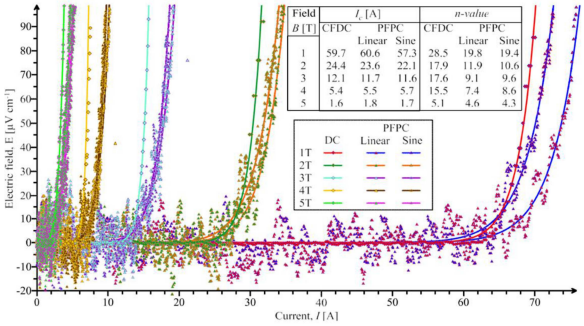


Fig. 13. $E$–$I$ curves recorded from the wire during the CF/DC and CB-PF/PS-PC measurements with two shapes of current ramp (Fig. 11). The inset table presents the $I_c$ and $n$-values obtained from each curve. However, measured critical current values are rather similar for CF/DC and Linear-CB-PF/PS-PC and a Sine-CB-PF/PS-PC (see Fig. 11) but the $n$-values (especially at lower flux densities) differ noticeably.

The resulting electric field vs. current response of the sample was finally processed by subtracting a linear fit to the low current behavior, to eliminate any slope in the signal. The superconducting transition can be described by (1) and curves calculated with this equation were fitted to the data points using the Levenberg–Marquardt method in the range of $E$ up to 100 $\mu$V/cm. The resulting $I_c$ and $n$-values based on a $E_c = 1$ $\mu$V/cm criterion are tabulated in Fig. 13. The amplitudes of the current pulses for each $B$ pulse were selected in such a way that the maximum $E$ (after corrections) from the sample at maximum current was close to 200 $\mu$V/cm for both the linear and sinusoidal current shapes. For the sinusoidal ramp, $I_c$ was therefore measured when the rate of a sample current change was decreasing to zero (with the current near the maximum).

### 4.3. Results and discussion

The $I_c$'s obtained by regression analysis of the $E$–$I$ curves from both the CF/DC and CB-PF/PS-PC techniques agree reasonably well, see Fig. 13. Linear and sinusoidal pulse shapes resulted in very similar estimates of $I_c$, with some systematic underestimation of $I_c$ in the low field range and overestimation in the high field range for the sinusoidal current shape. The noise level of $E$ without software averaging CB-PF/PS-PC measurement was on the level of 20 $\mu$V/cm and consequently it is likely that the measurements described in the previous section correspond to $E_c$ at least one order of magnitude higher than for the CF/DC technique. Adopting the same $E_c$ may therefore account for 10% $I_c(B)$ of the discrepancy between the results from the CB-PF/PS-PC and CF/DC techniques shown in Fig. 9. Clearly, when using the same $E_c$, some $I_c$ discrepancy remains but for example at 1 T the relative error between CF/DC and CB-PF/PS-PC is only −1.5% and 4% for linear and sinusoidal current ramps, respectively (Fig. 13). This error level is sufficiently low to attribute much of it to measurement uncertainties of the voltage, current and field in both the CF/DC and CB-PF/PS-PC systems.

The $I_c$ and $n$-value of the sample can be obtained from the $E$–$I$ curve by fitting a power-law (1). The analysis presented below assumes that the electric field signal in the $E$–$I$ curve obtained from CB-PF/PS-PC measurements contains three main components:

$$E_t(I, I_c, k, \eta) = E_i(k) + E_n(I, I_c, k) + E_\eta(I, k, \eta). \tag{2}$$

The total electric field $E_t$ is a function of $I = kt$, where $k$ and $t$ are the current ramp rate and time, respectively, $I_c$ — the critical current at constant $T$ and $B$ and $\eta$ — the viscous drag coefficient. In the CB-PF/PS-PC technique, usually the largest component is $E_i$ induced by the changing magnetic flux in the loop created by the sample and voltage contacts. By assuming that the contact wires enclose a rectangular area bounded by an outer radius $r_2$, this component can be calculated by the following equation:

$$E_i(k) = \frac{\mu_0}{2\pi} \ln\left(\frac{r_2}{a}\right), \tag{3}$$

where $a$ is the radius of the superconducting monofilament with an infinite length. Please note that $E_i$ is independent of $I$ and for constant $k$, $E_i$ is constant and can be subtracted from $E_t$. A second component of $E_t$ is $E_n$, induced by the changing flux inside the superconducting filament. In the simplest form and using the Bean model [11] (infinite $n$-value), $E_n$ is expressed by

$$E_n(I, k) = -\frac{\mu_0}{4\pi} \ln\left(1 - \frac{I}{I_c}\right). \tag{4}$$

The third component of $E_t$ in (2) is the viscous drag electric field $E_\eta$ which can be understood

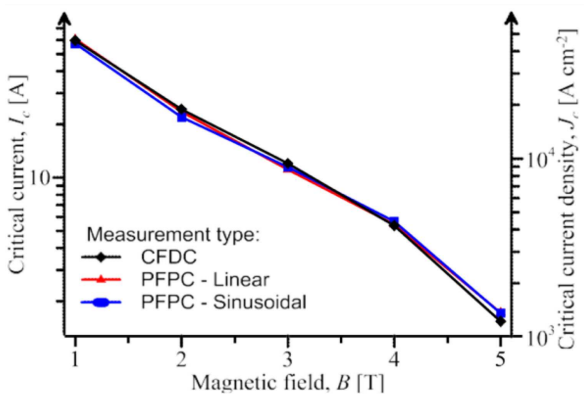


Fig. 14. The $I_c(B)$ and $J_c(B)$ obtained by the CF/DC and CB-PF/PS-PC methods.

from the dynamic equation of motion of vortices. This drag field can be expressed in a scalar form as [12, 13]:

$$F_L = F_p + F_\eta = J_c B + \eta \frac{B}{\Phi_0} \eta_{\Phi_0}. \tag{5}$$

Any remaining discrepancy might be due to the subtraction procedure itself. As expected, the electric field recorded from the sample during a current pulse without applied magnetic field contains the induced component resulting from the existence of a closed loop with the voltage taps: the equivalent loop size, $r_2$ as defined in (3) can be calculated as 8.3 mm. However, there is also an electric field component related to the behavior of the sample which is non-linear in current amplitude (see (4)). Although its value, even for the relatively high current ramp rates applied here, is very low, subtracting it from the measurements with both the pulsed current and magnetic field increasingly underestimates the sample electric field, especially above the transition, contributing to the lower $n$-values (Fig. 13). The $n$-values measured in CB-PF/PS-PC are much lower than those from CF/DC measurements but quite similar for both the sinusoidal and linear current pulse shapes. Such a behavior is very often, in the literature [14–16], associated with heating effects which affect the CFDC more than the PFPC measurements. Such an explanation is not satisfactory for the samples measured here in liquid helium and with relatively low transport current, and this issue will be discussed in Sect. 5.

The comparison of the $I_c$'s versus magnetic field (Fig. 14) obtained by CFDC and CB-PF/PS-PC shows very good agreement and proves that the refined measurement technique and data analysis are enough to improve accuracy, especially in the high field region. Some discrepancy still remains and the measurement procedure still requires a relatively large number of pulses in order to record all the voltages necessary for the subtraction procedure which — as discussed — is not perfect itself. Data processing, although it can be partly automated, is also relatively time-consuming in this case. Further, a refined method of critical current measurement with the PFPC technique will be described in which most of these issues are addressed.

## 5. CB-PF/PSS-PC measurements technique: stepwise current change

A CB-PF/PSS-PC measurement procedure using a pulsed current changed in a stepwise way is described. This procedure results in no need for subtracting induced voltage signals from the measured sample voltage. Use of the arbitrary waveform generator and KEPCO power supplies (Fig. 10) with a very impressive transient response allows great freedom in choosing the number of steps, the change of current and the change of current per step. From the observed transient response, it was estimated that the number of steps should not exceed 25: a larger number could result in the measured sample response being blurred by very rapid changes of current. In Fig. 15 the timing and amplitude changes of current shape used for this measurement are shown. This current shape has eight steps of equal duration, the first corresponding to half of the current amplitude $I_p/2$ and subsequent levels increasing by one-fourteenth of the current amplitude ($I_p/14$) until after 4 ms, $I_p$ is reached. To obtain a complete and continuous $E$–$I$ curve, many more current levels are necessary and this was achieved using a series of pulses with different amplitudes: an example is as shown in Fig. 16. It should be noted that not all the current pulses necessary to cover the range of current up to 92 A at 1 T are presented. The number of current pulses used for measurement at each field was in the range from 30 to 80. For measurements with higher amplitudes of pulsed magnetic field, the investigated current range is much smaller (smaller $I_c$) and for the same number of pulses the difference of levels in current pulses was decreasing. In Fig. 17, a signal averaging procedure is shown for the current pulse with an amplitude of 92 A for which the transient components are highest due to the large current steps.

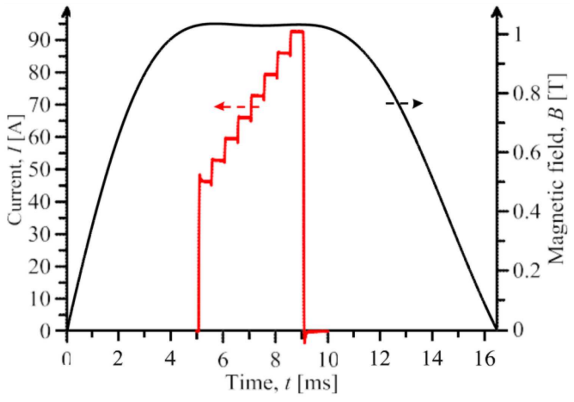


Fig. 15. Timing of the magnetic field and current pulses used for testing.

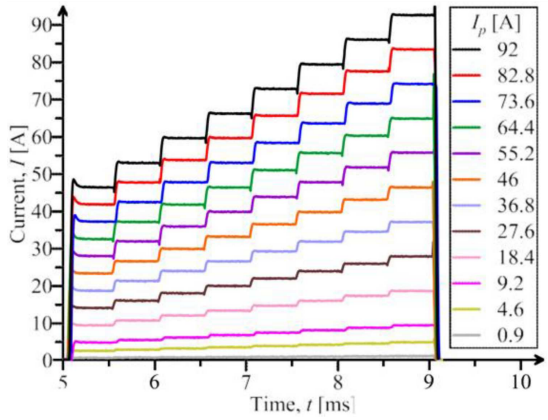


Fig. 16. Example of a series of current pulses with a variable amplitude used to cover the range of current levels from 0.45 A to 92 A.

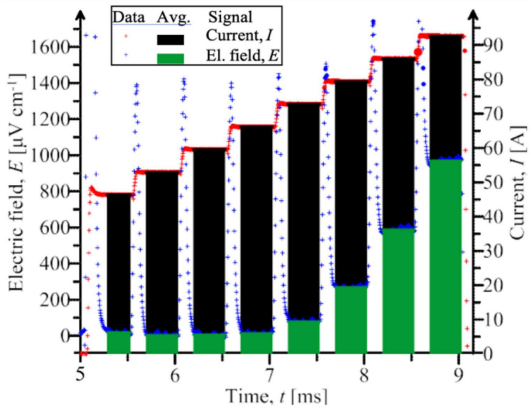


Fig. 17. Electric field (blue crosses, left ordinate) and current (red crosses, right ordinate) recorded during single magnetic field (not shown) and current pulses. The black line corresponds to averaging of the sample current, whereas the green line corresponds to averaging of electric field. Each symbol corresponds to a single data point.

The electric field signal contains very sharp peaks which correspond to the rapid current change between current levels.

These induced voltage peaks are ignored in data processing and the signals are averaged during the constant current (black line) and electric field (green line) periods. This corresponds to averaging over 63 data points or 0.25 ms and 85 data points or 0.34 ms, for the first and subsequent pulsed current levels (Fig. 17). It should be noted that with eight current steps, the sample electric field signal recorded during 4 ms consisted of 1000 points from which, due to the transient peaks, only 658 are used. It is certainly possible to use a rectangular current pulse with a constant amplitude over 4 ms and then conduct the averaging over almost all of the recorded points but to cover the whole current range this would require a lot of measurement time. This measurement procedure

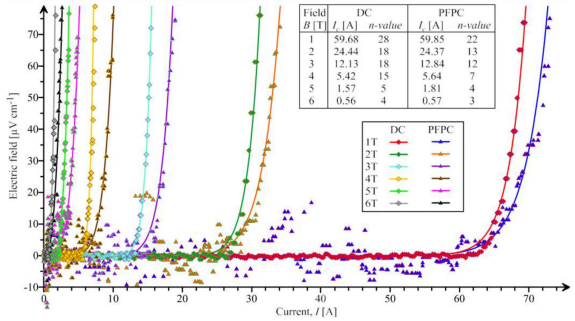


Fig. 18. $E$–$I$ curves recorded from the wire during constant field direct current (CF/DC) and pulse field pulse current (CB-PF/PSS-PC) measurements using stepwise current ramps (Fig. 15). The inset table presents the $I_c$ and $n$-values obtained from each curve.

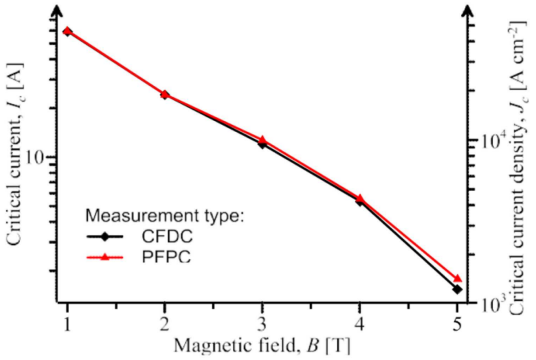


Fig. 19. The $I_c(B)$ ($J_c(B)$) obtained with CB-PF/PSS-PC, using stepwise current ramps and CF/DC methods.

and data processing produces data points of electric field vs. current which can be plotted (Fig. 18) without any additional correction. The agreement between the CB-PF/PSS-PC and CF/DC method is very good: the difference in measured $I_c$ for this wire is only 170 mA at 1 T and 10 mA at 6 T which correspond to −0.3% and −1.8% (Fig. 19). Some differences are, however, still clear in the shapes of the transitions to the resistive state. It is believed that viscous drag forces acting on vortices play a major role in producing this discrepancy.

### 5.1. Summary of the pulsed critical current measurements

A refinement of the CB-PF/PSS-PC technique for $I_c$(B) measurement has been demonstrated, in which $I_c$ can be determined at a chosen electric field criterion. The resulting $I_c$ and $n$-value are in good agreement with CF/DC results, with a small dependence on the current pulse shape, with most of the differences caused by the much higher ramp rates in the CB-PF/PSS-PC technique. A linear current ramp is not dramatically better than a sinusoidal one but this and other interesting shapes of current, like a triangular current pulse to record

the voltage response during increasing and decreasing current from the sample and then apply averaging, could be of interest in some cases, as reported in [17]. The current source used in the present work restricts the range of currents which can be achieved but provides a very high degree of flexibility in controlling the current pulse shape and duration. This feature was exploited by using stepwise current change which so far gives the best results and much simplified data analysis. The results are also less noisy due to extensive averaging of the measurement points. Still the noise level in the data could be improved by using a low noise amplifier in the voltage recording channel. When this is improved, it would be desirable to conduct a systematic study of the effect of current ramp rate on measurements but the constrained measurement time due to the duration of the magnetic field pulse suggests that such experiments should ideally be performed in a superconducting magnet.

The superconductor during such a rapid current change does not have time to be in magnetic equilibrium and this strongly affects the results. Due to a flux creep in the superconductor it takes a finite time for the flux to diffuse into the sample. Therefore, the measured $I_c$ will always depend on the time and length scales of the experiment. This influence can in principle be calculated and the results corrected if a complete understanding of the influencing factors is known. The results presented here were obtained in nearly isothermal conditions due to efficient cooling by a liquid cryogen. However, the pulse current methods are of particular interest when the samples are cooled by conduction or by gaseous cooling mediums, where the energy deposited by the Joule heating is required to be minimised in order to maintain conditions close to isothermal or even prevent the sample from irreversible thermal degradation [18].

## 6. Conclusions

The pulsed field pulsed current critical current measurement method has been refined, using a capacitor bank discharge pulse field/power supply stepwise pulse current CB-PF/PSS-PC, allowing a standard electric field criterion to be applied and $n$-values to be measured. The results are in very good agreement with the conventional CF/DC method and are only affected by vortex dynamics during viscous movement in the flux flow region. A need for a less noisy electric field signal is emphasized, as it would allow for investigation of the voltages caused by the flux movement in the flux creep regime during the current pulse through the sample. This and experiments which would allow for longer time measurement to investigate the current ramp effect are recommended as future work which would lead to better understanding of this rapid and economical measurement technique.

## References


[1] Z. Cai, R.H. Clarke, B.A. Glowacki, W.J. Nuttall, N. Ward, *Resourc. Policy* **35**, 77 (2010).

[2] W.J. Nuttall, Z. Cai, B.A. Glowacki, N. Kazantizis, R.H. Clarke, in: Series: Routledge Explorations in Environmental Economics, Eds. W.J. Nuttall, R. Clarke, B.A. Glowacki, Routledge, Taylor & Francis, Oxford, UK 2012, p. 157.

[3] B.A. Glowacki, A. Gilewski, K. Rogacki, A. Kursumovich, J.E. Evetts, H. Jones, R. Henson, O. Tsukamoto, *Physica C* **384**, 205 (2003).

[4] K. Rogacki, A. Gilewski, J. Klamut, H. Jones, M. Newson, B.A. Glowacki, *Supercond. Sci. Technol.* **15**, 1151 (2002).

[5] V. Stehr, K.S. Tan, S.C. Hopkins, B.A. Glowacki, A. De Keyser, L. Van Bockstal, J. Deschagt, *J. Phys. Conf. Series* **43**, 682 (2006).

[6] S. Krosny, M. Woźniak, S.C. Hopkins, M.A. Stępień, B. Grzesik, B.A. Glowacki, *J. Phys. Conf. Series* **234**, 022019 (2010).

[7] L. Van Bockstal, A. De Keyser, J. Deschagt, S.C. Hopkins, B.A. Glowacki, *Physica C* **460**, 839 (2007).

[8] M. Woźniak, K.L. Juda, S.C. Hopkins, D. Gajda, B.A. Glowacki, *Supercond. Sci. Technol.* **26**, 105008 (2013).

[9] W. Suski, T. Palewski, V.I. Nizhankovskii, J. Klamut, *J. Phys. Conf. Ser.* **51**, 603 (2006).

[10] Kepco Inc. Operators manual for BOP series power supplies, www.kepcopower.com.

[11] C.P. Bean, *Phys. Rev. Lett.* **8**, 250 (1962).

[12] G. Blatter, M.V. Feigel'man, V.B. Geshkenbein, A.I. Larkin, V.M. Vinokur, *Rev. Mod. Phys.* **66**, 1125 (1994).

[13] H. Fujishiro, T. Hiyama, T. Naito, T. Tateiwa, Y. Yanagi, *Mater. Sci. Eng. B* **151**, 95 (2008).

[14] A. Stenvall, I. Hiltunen, J. Jarvela, A. Korpela, J. Lehtonen, R. Mikkonen, *Supercond. Sci. Technol.* **21**, 065012 (2008).

[15] I. Hiltunen, J. Lehtonen, R. Mikkonen, A. Stenvall, *Physica C* **469**, 1987 (2009).

[16] I. Hiltunen, J. Lehtonen, A. Stenvall, R. Mikkonen, *IEEE Trans. Appl. Supercond.* **20**, 1597 (2010).

[17] C.A. D'Ovidio, D.A. Esparza, M.T. Malachevsky, *Physica C* **372-376**, 162 (2002).

[18] K.W. See, X. Xu, J. Horvat, C.D. Cook, S.X. Dou, *Supercond. Sci. Technol.* **24**, 105009 (2011).